in silico Plants Vol. 3, No. 1, pp. 1–19
doi:10.1093/insilicoplants/diab001
Advance Access publication 08 January 2021
Special Issue: Linking Crop/Plant Models and Genetics
Original Article

in silico Plants

OXFORD

Integrating crop growth models with remote sensing for predicting biomass yield of sorghum

Kai-Wei Yang[1], Scott Chapman[2,3], Neal Carpenter[1], Graeme Hammer[4], Greg McLean[4], Bangyou Zheng[3], Yuhao Chen[5], Edward Delp[5], Ali Masjedi[6], Melba Crawford[1,6], David Ebert[5], Ayman Habib[6], Addie Thompson[1,7], Clifford Weil[1] and Mitchell R. Tuinstra[1*]

[1]Department of Agronomy, Purdue University, 915 West State Street, West Lafayette, IN 47907, USA
[2]School of Agriculture and Food Sciences, The University of Queensland, Gatton, QLD 4343, Australia
[3]CSIRO Agriculture and Food, Queensland Biosciences Precinct, 306 Carmody Road, St Lucia, QLD 4067, Australia
[4]Queensland Alliance for Agriculture and Food Innovation (QAAFI), The University of Queensland, Brisbane, QLD 4072, Australia
[5]School of Electrical and Computer Engineering, Purdue University, 465 Northwestern Avenue, West Lafayette, IN 47907, USA
[6]Lyles School of Civil Engineering, Purdue University, 550 Stadium Mall Drive, West Lafayette, IN 47907, USA
[7]Plant Soil and Microbial Sciences Department, Michigan State University, 1066 Bogue Street, East Lansing, MI 48824, USA
*Corresponding author's e-mail address: mtuinstr@purdue.edu

Guest Editor: Xinyou Yin
Editor-in-Chief: Stephen P. Long

Citation: Yang K-W, Chapman S, Carpenter N, Hammer G, McLean G, Zheng B, Chen Y, Delp E, Masjedi A, Crawford M, Ebert D, Habib A, Thompson A, Weil C, Tuinstra MR. 2021. Integrating crop growth models with remote sensing for predicting biomass yield of sorghum. *In Silico Plants* **2021**: diab001; doi: 10.1093/insilicoplants/diab001

ABSTRACT

Plant phenotypes are often descriptive, rather than predictive of crop performance. As a result, extensive testing is required in plant breeding programmes to develop varieties aimed at performance in the target environments. Crop models can improve this testing regime by providing a predictive framework to (i) augment field phenotyping data and derive hard-to-measure phenotypes and (ii) estimate performance across geographical regions using historical weather data. The goal of this study was to parameterize the Agricultural Production Systems sIMulator (APSIM) crop growth models with remote-sensing and ground-reference data to predict variation in phenology and yield-related traits in 18 commercial grain and biomass sorghum hybrids. Genotype parameters for each hybrid were estimated using remote-sensing measurements combined with manual phenotyping in West Lafayette, IN, in 2018. The models were validated in hybrid performance trials in two additional seasons at that site and against yield trials conducted in Bushland, TX, between 2001 and 2018. These trials demonstrated that (i) maximum plant height, final dry biomass and radiation use efficiency (RUE) of photoperiod-sensitive and -insensitive forage sorghum hybrids tended to be higher than observed in grain sorghum, (ii) photoperiod-sensitive sorghum hybrids exhibited greater biomass production in longer growing environments and (iii) the parameterized and validated models perform well in above-ground biomass simulations across years and locations. Crop growth models that integrate remote-sensing data offer an efficient approach to parameterize larger plant breeding populations.

KEYWORDS: APSIM; bioenergy sorghum; extinction coefficient; high-throughput phenotyping; LAI; photoperiod-sensitive sorghum; radiation use efficiency; scenario simulation.

1. INTRODUCTION

1.1 Importance of forage sorghum in rainfed environments

Sorghum (*Sorghum bicolor*) is commercially important in semi-arid environments due to its substantial heat and drought tolerance. Grain sorghum is the fifth most important cereal in global production with over 57 million tonnes of grain produced on 40 million ha in 2017 (FAOSTAT). Sorghum is also an important forage and sugar crop and can be utilized to produce plant-based biofuels including starch from sorghum grain, sugar from sweet-stemmed sorghum and cellulose from plant leaves and stems. In the USA, almost one-third of the sorghum grain crop is processed through grain-based ethanol production systems. Limited quantities of sugar-based and cellulose-based biofuel are produced currently, but these are considered important feedstocks for the future, minimizing direct competition with food production (Tilman *et al.* 2006; Rubin 2008).

Biomass sorghums can reach heights of 4–5 m with biomass yields maximized by high crop growth rates throughout the available growing season (Rocateli *et al.* 2012). When planted at high density, commercial sorghum hybrids exhibit a diversity of plant and canopy types to quickly reach maximum radiation interception (Rooney *et al.* 2007; Olson *et al.* 2012; Gill *et al.* 2014; Truong *et al.* 2017). Total leaf number was found to be highly correlated with length of vegetative period. Hence, early maturing sorghum has fewer leaves and lower biomass production (Sieglinger 1936). In contrast, at high latitudes, spring-sown photoperiod-sensitive sorghum hybrids exhibit extended vegetative periods resulting in high biomass yields. Moreover, since sorghum exhibits better drought tolerance during vegetative growth stages, the longer period of vegetative growth results in better drought tolerance or drought avoidance in rainfed environments (Rooney *et al.* 2007).

1.2 High-throughput phenotyping methods potentially facilitate the measurement of canopy and crop growth through the entire cropping season

Marker-assisted selection (MAS), next-generation sequencing (NGS) technologies and data analytics pipelines have contributed to the implementation of genome-wide association studies (GWAS), genomic diversity studies, genetic linkage analyses, molecular marker discovery and genomic selection in large-scale plant breeding programmes (He *et al.* 2014). Although genomic technologies are developing quickly, understanding the biological determinants of quantitative phenotype variation remains the central challenge of modern genetic analysis. New, high-throughput phenotyping (HTP) technologies are expected to be the next step in developing association mapping, gene discovery and developing predictive genomic selection models in crop improvement (Cobb *et al.* 2013).

High labour costs often constrain crop breeding programmes to single measurements of final yield in diverse testing environments over multiple seasons. This bottleneck in field phenotyping has driven intense interest in applying remote-sensing technologies to field crop monitoring (Furbank and Tester 2011). Remote sensing of crops includes passive and active sensing of plants to acquire and interpret data to extract information about features, objects and classes in the area of interest (Konare *et al.* 2003). Data are processed through an analysis pipeline to calibrate and convert digital data into interpretable information (Campbell 2006). For example, the dynamics of canopy cover influence the pattern of crop growth rate and eventual yield. Remote-sensing images acquired by unmanned aerial vehicles (UAVs) can be used directly for large-scale estimation of leaf coverage and are key components of high-throughput field phenotyping (Duan *et al.* 2014, 2017; Gouache *et al.* 2016; Stanton *et al.* 2017; Zhang *et al.* 2017; Masjedi *et al.* 2018; Ribera *et al.* 2018).

Multiple remote-sensing approaches focused on quantifying variations in canopy cover and its dynamics have been investigated. An image-based workflow to monitor the growth and development of the wheat canopy dynamically using RGB cameras was developed by Duan *et al.* (2016). Similarly, Guo *et al.* (2017) evaluated the ground coverage ratio of rice from a large number of RGB images under variable field conditions. Light Detection and Ranging (LiDAR) has also been used to estimate canopy cover and above-ground biomass (Jimenez-Berni *et al.* 2018). Masjedi *et al.* (2019) introduced a strategy that incorporates multi-sensor time series data, environmental inputs and use Recurrent Neural Networks to predict sorghum biomass. Blancon *et al.* (2019) reported a high-throughput, model-assisted method for quantifying green leaf area (GLAI) dynamics in maize using multispectral imagery. Zhou *et al.* (2019) used an image-segmentation method based on machine learning to extract relatively accurate coverage information from RGB images. All of these approaches utilize remote-sensing technology to collect canopy-based phenotypes. However, interpreting dynamics of change is not easily done in empirical models.

1.3 Crop growth models

Dynamic crop growth modelling and simulation have become accepted tools for agricultural research (e.g. WOFOST (Diepen *et al.* 1989), DSSAT (Jones *et al.* 2003), APSIM (Keating *et al.* 2003; Holzworth *et al.* 2018), CROPSYST (Stöckle *et al.* 2003), EPIC (Williams *et al.* 1983, 1989)) (Bouman *et al.* 1996; Jones *et al.* 2017). Unlike purely statistical approaches, these models have functions that respond to external drivers and how those responses affect other components in the system (Wallach *et al.* 2018). Well-developed crop growth models as well as HTP approaches have been developed in recent years (Demarez *et al.* 2008; Casa *et al.* 2010; Baret *et al.* 2018; Blancon *et al.* 2019; Jiang *et al.* 2019; Parent *et al.* 2019); however, strategies that accommodate crop growth models as part of HTP pipelines have not been thoroughly explored.

Agricultural Production Systems sIMulator (APSIM) is a biophysical simulation model for cropping systems that was designed to predict the dynamics of crop growth, including biomass and grain yield, in response to climate and management conditions (Keating *et al.* 2003). Agricultural Production Systems sIMulator incorporates a generic crop model that utilizes a library of routines for simulating crop growth and development processes (Wang *et al.* 2002) and has been used to investigate diverse questions related to food security, climate change adaptation and mitigation, simulation of gene expression and multi-trial simulation (Holzworth 2014).

In the investigation of biomass growth in crops like biomass sorghum, the key physiological processes are phenology, leaf area development and crop growth rate as affected by weather and soil

conditions. Simulated phenology in APSIM is based on thermal time elapsed in growth stages. Thermal time is calculated from a piecewise linear function of the mean air temperature, depending on base, optimum and maximal temperatures, which are 11, 30 and 42 °C for sorghum, respectively (Hammer *et al.* 1993). Panicle initiation (conversion of the meristem from production of vegetative initials to reproductive initials) is triggered at a genotype-specific thermal time, which can be further influenced by a genotype-specific photoperiod response. The accumulated thermal time between emergence and simulated panicle initiation determines the value of the total leaf number when divided by the plastochron (°Cd per leaf), period between the appearance of two successive leaf primordia. Leaves are expanded at a rate determined by the phyllochron (°Cd per leaf), period between the appearance of two successive leaves, and thus the product of total leaf number and phyllochron determines the thermal time to reach flag leaf stage (°Cd) (Hammer *et al.* 2010). The duration of growth stages such as flag leaf to anthesis, anthesis to start of grain filling and start to end of grain filling are also simulated in the model by accumulation of thermal time to reach genotype-specific target values (Muchow and Carberry 1990; Hammer and Muchow 1994; Ravi Kumar *et al.* 2009).

Canopy development is simulated based on the relationship between total plant leaf area (TPLA) and thermal time. Total plant leaf area accounts for the number of fully expanded leaves, size of each leaf and tiller number (Hammer *et al.* 1993, 2010). The model provides flexibility to simulate canopy development using other options such as leaf size distribution (Carberry *et al.* 1993; van Oosterom *et al.* 2001; Hammer *et al.* 2010) or the extension rate of each leaf (Hammer *et al.* 2010; Chenu *et al.* 2018). In the standard version of APSIM, the above-ground dry biomass accumulation is simulated as the minimum of light-limited or water-limited growth, then biomass is partitioned in different ratios to plant parts depending on the plant developmental stages through founded functions (Hammer *et al.* 2010).

1.4 Bioenergy sorghum

The objectives of this study are to develop a crop model for biomass sorghum that can predict seasonal biomass production of diverse hybrids over multiple seasons at different locations by combining HTP and crop growth models. Canopy cover estimated from RGB images was used to estimate key parameters describing leaf cover dynamics, light interception and radiation use efficiency (RUE). Other canopy properties were derived as outputs of the APSIM model. This method provides a new approach for understanding the adaptation of biomass sorghum and its interaction with the environment to identify trait targets for plant breeding.

2. MATERIALS AND METHODS

2.1 Genotypes and field management

A set of 18 sorghum hybrids (*S. bicolor*) (Table 1) were grown in 2015, 2017 and 2018 at the Agronomy Center for Research and Education (ACRE) of Purdue University in West Lafayette, IN, USA. Daily solar radiation, maximum and minimum temperatures and precipitation were recorded at the experimental site. Field trials were conducted each year using a randomized complete block design with four replicates. The hybrid entries were evaluated in 12-row plots with 76 cm spacing between rows measuring 3.81 m long. Seeds were sown at 30-mm depth on 19 May in 2015, 16 May in 2017 and 8 May in 2018 with emerged densities as shown (Table 1). Weeds and pests were controlled as required and there was negligible pest damage to the photosynthetic leaf surface throughout growth.

2.2 Ground validation studies

Ground-reference data from trials conducted in 2018 were used to parameterize the APSIM model. Plant population density was determined from row 2 and row 3 of each 12-row plot at 31 days after sowing (DAS). Days to flowering were measured as the number of days from sowing to when 50 % of the panicles in the plot were at 50 % anthesis. Plant height was measured after flowering.

Destructive harvests at four different stages of development were used to determine biomass yields; leaf, stem, tiller and panicle weights of individual plants; and leaf size distribution. Four plants were harvested manually from plot row 11 on 7 June (31 DAS), two plants from plot rows 8 and 9 on 25 June (49 DAS), two plants from plot rows 5 and 6 on 12 July (66 DAS) and two plants from plot rows 2 and 3 on 9 August (94 DAS). After harvesting, each plant was dissected to determine the weight of the collared leaves, leaves that had not fully emerged, stems, tillers and panicle fractions. Leaves were removed from each plant in order and scanned individually to determine leaf size distribution using a LI-3100C Leaf Area Meter (LI-COR, Lincoln, NE, USA). The final tiller number was estimated from the tiller dry weight and total plant dry weight. Percent moisture of each plant was determined from the combined fresh weights and, later, dry weights of all fractions from each plant.

Repeated non-destructive measurements of plant development were also made during the vegetative period including the number of fully expanded leaves (collared leaves) of four tagged plants in rows 2 and 3 of each plot. Collection dates were 7 June (31 DAS), 19 June (43 DAS), 28 June (52 DAS), 5 July (59 DAS), 11 July (65 DAS) and 26 July (80 DAS). The final leaf numbers were the maximum value of leaf collar counts of each plot across dates. Final tiller number per plant was determined on 12 July (66 DAS). The average leaf biomass fraction and specific leaf weight (SLW) were used to compute leaf area and leaf area index (LAI) for each plot and sampling date.

Total biomass yields were measured in each plot on 7 June (31 DAS), plot rows 8 and 9 on 25 June (49 DAS), plot rows 5 and 6 on 12 July (66 DAS) and plot rows 2 and 3 on 9 August (94 DAS); one replicate was not harvested at 49 DAS due to inclement weather. On 7 June (31 DAS), a 2-m section of row segment 11 was hand-harvested, weighed and dried to compare fresh weights and dry weights. For the next three harvest dates, the entire 2-row segment of each plot was harvested with a Wintersteiger Cibus 2-row Biomass Harvester (Wintersteiger Inc., Salt Lake City, UT, USA). After harvesting a plot, ~500 g of the shredded plant material from each plot was taken to determine fresh weight, dry weight and moisture content. For the mechanically harvested plots, a 0.614-kg fresh weight correction factor was added back to the biomass estimate of each plot to account for the short stem segments that were left behind after machine harvesting. At the last sampling date (94 DAS), several plots were lodged and could not be harvested.

Table 1. Details of the types and observed data for 18 hybrids in central-west Indiana from May to October. The value in a cell is mean plus minus standard deviation and the results of LSD test. **Significant at the 0.001 probability level. †PH, seeds from Pioneer Hi-Bred; RS, seeds from Richardson Seeds; SP, seeds from Sorghum Partners.

Genotype†	Type	2015 plant density	2017 plant density	2018 plant density	2017 flowering date
			stand count per m^2		DAS
PH 849F	Forage sorghum	15.5 ± 1.3abcde	15.9 ± 1.3def	18.3 ± 0.8defg	72.8 ± 9.2ef
PH 877F	Forage sorghum	16.1 ± 1.6abc	19.5 ± 1.7a	19.6 ± 0.5ab	66.3 ± 1.9gh
RS 327x36 BMR	Forage sorghum	15.6 ± 1.1abcd	18.5 ± 2.0abc	19.1 ± 0.8abcde	91.0 ± NAc
RS 341x10	Food grade	15.5 ± 0.8abcde	16.7 ± 1.3cde	17.4 ± 1.1g	68.8 ± 0.5fgh
RS 366x58	Food grade	12.9 ± 1.8f	12.7 ± 0.3g	15.9 ± 0.7h	77.3 ± 3.1de
RS 374x66	Forage sorghum	14.2 ± 1.2cdef	13.9 ± 0.6fg	17.5 ± 0.9fg	75.0 ± 4.8def
RS 392x105 BMR	Forage sorghum	16.4 ± 1.0ab	17.8 ± 1.9abcd	19.6 ± 0.7abc	91.0 ± 0.0c
RS 400x38 BMR	Sorghum-sudangrass	16.3 ± 0.9ab	17.7 ± 1.8abcd	18.6 ± 1.0bcdef	74.8 ± 1.9def
RS 400x82 BMR	Sorghum-sudangrass	13.7 ± 1.3def	14.1 ± 0.8fg	15.0 ± 0.8h	76.0 ± NAdef
SP HIKANE II	Forage sorghum	15.5 ± 0.6abcde	18.7 ± 1.6abc	20.1 ± 0.7a	74.0 ± 2.6def
SP NK300	Forage sorghum	16.8 ± 2.1a	19.4 ± 2.0ab	19.4 ± 1.0abcd	79.3 ± 1.0d
SP NK5418	Grain sorghum	15.4 ± 1.0abcde	18.7 ± 1.2abc	19.4 ± 0.5abcd	68.0 ± 1.0fgh
SP NK8416	Grain sorghum	13.5 ± 1.7ef	15.2 ± 2.2ef	15.4 ± 1.1h	79.3 ± 1.7d
SP Sordan 79	Forage sorghum	14.8 ± 0.7abcdef	18.2 ± 2.3abcd	17.7 ± 0.8fg	71.0 ± 2.3fg
SP Sordan Headless	Forage sorghum photoperiod-sensitive	15.1 ± 1.2abcde	18.0 ± 1.3abcd	18.5 ± 0.4cdefg	138.0 ± 0.0a
SP SS405	Forage sorghum	14.2 ± 1.3cdef	17.4 ± 0.8abcde	18.1 ± 0.5efg	NA
SP Trudan 8	Forage sorghum	12.9 ± 1.6f	17.1 ± 2.3bcde	15.2 ± 0.3h	63.7 ± 0.6h
SP Trudan Headless	Forage sorghum photoperiod-sensitive	14.5 ± 2.8bcdef	16.6 ± 2.8cde	15.2 ± 0.8h	131.5 ± 7.5b
Degrees of freedom		53	54	54	43
Mean		15.0	17.0	17.78	82.6
Coefficient of variation		9.6	9.9	4.4	4.5
P-value from ANOVA		3.3e-03	1.2e-06	<2e-16	<2e-16
Significance		**	**	**	**

2.3 Ground validation data from 2015 and 2017

Replicated trials conducted in 2015 and 2017 were used to validate the parameterized APSIM models for each hybrid. Total above-ground biomass was measured by manual sampling and by machine harvesting. Manual sampling was conducted at 65 and 93 DAS in 2015, and 42, 63, 84 DAS in 2017 by harvesting plants from three 1-m sections of row in rows 5–8 of the 12-row plot. Plant count and biomass fresh weight and dry weight were measured for each sample. An individual plant from each sample was dissected to measure leaf, stem, tiller and panicle weights. The leaf sizes were determined using ImageJ, an open source software package developed by NIH for the analysis of scientific images (Schneider *et al.* 2012). The leaves were laid on a white board in leaf order from top to bottom. RGB images of the leaves were acquired using a Cannon EOS 6D camera with a Canon 35-mm lens under a white light source and ~1.5 m height. Leaves were segmented by thresholding in HSB (Hue, Saturation, Brightness) colour space with four thresholds. Total leaf area per plant and plant stand information were used to calculate the LAI. A Wintersteiger Cibus 2-row Biomass Harvester (Wintersteiger Inc., Salt Lake City, UT, USA) was also used to mechanically harvest plants from plot rows 10 and 11 on 25 August 2015 (99 DAS) and 31 July 2017 (77 DAS) and from plot rows 2 and 3 on 27 September 2017 (135 DAS) as described above.

2.4 Remote-sensing data collection

Remote-sensing data were used to measure canopy cover for each plot. RGB images were collected in 2017 and 2018 using a DJI Matrice M600 Pro UAV as a platform, equipped with an APX-15 V2 as the GNSS (Global Navigation Satellite System)/INS (Inertial Navigation System) unit for direct geo-referencing. Images were collected using a Sony Alpha 7R (ILCE-7R) camera with a Sony 35-mm lens at a height of 50 m, resulting in a ground sampling distance of 0.7 cm. Spatial and temporal calibration of the imaging systems in this study were done by methods described in Ravi *et al.* (2018). The RGB images were collected in 2017 on 6 June (22 DAS), 21 June (37 DAS), 28 June (44 DAS), 5 July (51 DAS), 11 July (57 DAS), 17 July (63 DAS), 25 July (71 DAS), 2 August (79 DAS), 8 August (85 DAS), 16 August (93 DAS) and 30 August (107 DAS). RGB images were taken in 2018 on 16 May (9 DAS), 22 May (15 DAS),

2018 flowering date	2015 final dry biomass	2017 final dry biomass	2018 final dry biomass	2015 max height	2017 max height	2018 max height
		g m^{-2}			cm	
74.0 ± 4.0ef	1670 ± 194bc	2258 ± 382cde	2040 ± 111abc	244.6 ± 10.4def	242.5 ± 29.7de	273.8 ± 11.1bcd
66.8 ± 1.7gh	1497 ± 72cde	2217 ± 448.7cde	2006 ± 187abcd	265.0 ± 7.9c	224.0 ± 52.8ef	294.7 ± 13.5ab
83.8 ± 12.5d	1343 ± 269def	2245 ± 401cde	1645 ± 118defg	255.8 ± 12.7cde	246.2 ± 19.7de	250.0 ± 9.6d
65.5 ± 1.3gh	973 ± 82g	1465 ± 191h	1138 ± 17h	77.5 ± 1.6j	82.7 ± 1.9i	126.0 ± 1.8h
73.8 ± 2.1ef	1139 ± 85fg	1939 ± 160efg	1366 ± 173gh	123.5 ± 8.2i	139.3 ± 7.0h	153.3 ± 9.4g
69.8 ± 2.1efg	1634 ± 143bc	2049 ± 346defg	1988 ± 211abcd	263.1 ± 21.2cd	264.7 ± 8.9cd	263.9 ± 3.0cd
90.0 ± 0.0c	1117 ± 99fg	2318 ± 358bcd	1563 ± 196efg	163.0 ± 5.8h	203.4 ± 31.2fg	190.5 ± 13.5f
73.0 ± 1.4ef	1151 ± 148fg	1962 ± 102defg	1516 ± 55fgh	190.1 ± 11.0g	220.9 ± 7.3ef	216.5 ± 3.6e
104.0 ± 5.7b	1248 ± 305efg	2128 ± 59cdefg	1569 ± 403efg	242.6 ± 6.0def	191.7 ± 27.7g	202.8 ± 6.4ef
70.3 ± 1.3efg	1607 ± 237bc	2230 ± 372cde	2080 ± 203abc	239.4 ± 14.8ef	244.9 ± 6.0de	254.5 ± 30.1d
75.3 ± 3.3e	1570 ± 232bcd	2140 ± 290cdef	1919 ± 188bcd	180.0 ± 10.9gh	189.4 ± 5.0g	189.6 ± 13.1f
65.3 ± 1.9gh	1069 ± 94g	1754 ± 164gh	1210 ± 170h	66.8 ± 2.8j	73.8 ± 5.2i	116.0 ± 1.8h
70.3 ± 1.3efg	1183 ± 151fg	1929 ± 222efg	1364 ± 310gh	125.1 ± 9.6i	128.1 ± 5.9h	167.4 ± 8.9g
69.3 ± 2.9fg	1795 ± 134ab	1942 ± 111efg	2209 ± 221ab	291.0 ± 17.4b	261.4 ± 15.1cd	307.5 ± 1.1a
NA	1525 ± 217cde	3117 ± 98a	1882 ± 218cde	240.9 ± 20.7ef	297.6 ± 7.4b	257.8 ± 13.5d
108.0 ± 0.0b	1976 ± 70a	2466 ± 299bc	2288 ± 339a	338.5 ± 28.7a	342.0 ± 19.5a	296.0 ± 13.8ab
62.8 ± 0.5h	1523 ± 319cde	1803 ± 104fgh	1834 ± 300cdef	227.1 ± 11.4f	200.8 ± 18.7fg	287.7 ± 1.7abc
120.0 ± NAa	1628 ± 165bc	2634 ± 191b	1766 ± 66cdef	251.1 ± 11.8cde	277.3 ± 15.8bc	262.3 ± 30.1d
44	53	53	47	53	52	30
75.1	1427	2143	1777	209.8	212.2	224.1
5.2	13	12	13	6.5	9.0	5.8
<2e-16	1.0e-10	5.4e-09	1.3e-08	<2e-16	<2e-16	<2e-16
**	**	**	**	**	**	**

29 May (22 DAS), 4 June (28 DAS), 11 June (35 DAS), 20 June (44 DAS), 27 June (51 DAS), 2 July (56 DAS), 11 July (65 DAS), 18 July (72 DAS), 23 July (77 DAS), 1 August (86 DAS) and 6 August (91 DAS). The RGB images were collected in 2015 using a DJI Phantom 2 platform, and a GoPro Hero3+ camera at a height of 15 m, with ground sampling distance of 0.7 cm. The images were acquired on 15 June (28 DAS), 26 June (39 DAS), 6 July (49 DAS), 15 July (58 DAS) and 25 July (68 DAS).

Orthomosaics were obtained using modified Structure from Motion (SfM) strategies introduced in He *et al.* (2018) with ground control targets, and then used to identify the coordinates of the plots and row segments. While multiple photos may have overlapping plot coverage, the image coordinates for the same row segment vary from photo to photo. Row segments at the image border suffer more lens and perspective distortion than the row segments at the photo centre, which will have a big impact on canopy cover calculation. Therefore, the photo where the plot is closest to the centre of the image was used for canopy cover estimation. Each row segment was defined by a rectangle whose dimensions were 0.76 m × 3.81 m on average, and then 0.4 m was trimmed from each end of the row to minimize effects of the alley between plots. The canopy cover was estimated for rows 2 and 3 as the ratio of vegetative to non-vegetative pixels within the box, using segmentation methods described previously (Ribera *et al.* 2018) and canopy cover for each plot taken as the average of the two rows.

2.5 Agricultural Production Systems sIMulator

Weather data, soil data, field management and sorghum physiological parameters were used to parameterize the APSIM model for West Lafayette. Weather data included daily solar radiation (MJ), maximum and minimum temperatures (°C) and precipitation (mm). Field management parameters included sowing date, sowing depth and plant density (Table 1). The sorghum physiological parameters included observed parameters (final leaf number, final tiller number, maximum leaf area (m^2) and maximum leaf multiplier) and derived parameters (extinction coefficient of canopy (k) and RUE (g MJ^{-1})) determined from the 2018 data set (Table 2, see explanation of computation of k and RUE below).

2.6 Model calibration

An R pipeline for APSIM parameters calculation was developed to process the 2018 data set. The input data included of weather data and sorghum physiological parameters by plot. Weather data were comprised of maximum daily temperature, minimum daily temperature, precipitation and solar radiation. The sorghum physiological parameters for APSIM: observed leaf number, final tiller number, two leaf size distribution parameters, observed canopy cover and observed biomass, were extracted after spatial analysis of the variable values using spline fits (Rodríguez-Álvarez *et al.* 2018). Two leaf size distribution parameters, maximum leaf area (aMaxI) and maximum leaf multiplier (aX0) were determined for each hybrid. The leaf size functions were computed as follows (Carberry *et al.* 1993; Chenu *et al.* 2008):

$$a\text{Max} = a\text{MaxI}$$

$$\textit{Individual Leaf Size } (cm^2) = a\text{Max} \times \exp(a \times (\text{Leaf number} - \text{Largest leaf position})^2 + b \times (\text{Leaf number} - \text{Largest leaf position})^3) \times 100;$$

The factor 100 is a percentage of the maximum leaf size;

$$\text{Largest leaf position} = a\text{X0} \times \text{Final leaf number (FLN)};$$

FLN is counted along the stem upwards;

Table 2. 2018 parameters from the pipeline calculating derived parameters based on observed parameters. *K* for extinction coefficient and RUE for radiation use efficiency.

Genotype	*K*	RUE (g MJ^{-1})
PH 849F	0.57	1.47
PH 877F	0.98	1.53
RS 327x36 BMR	0.35	1.36
RS 341x10	0.46	1.15
RS 366x58	0.58	1.15
RS 374x66	0.48	1.60
RS 392x05 BMR	0.44	1.29
RS 400x38 BMR	0.46	1.27
RS 400x82 BMR	0.65	1.28
SP HIKANE II	0.54	1.61
SP NK300	0.84	1.40
SP NK5418	0.79	0.97
SP NK8416	0.55	1.10
SP Sordan 79	0.69	1.64
SP Sordan Headless	0.38	1.40
SP SS405	0.35	1.70
SP Trudan 8	1.43	1.44
SP Trudan Headless	0.38	1.40

$$a = a_0 - \exp(a_1 * \text{FLN});$$

$$b = b_0 - \exp(b_1 * \text{FLN});$$

$$a_0 = -0.009 \quad a_1 = -0.2$$
$$b_0 = 0.0006 \quad b_1 = -0.43$$

Using the leaf size function, the largest leaf area and the position multiplier of this leaf within the whole plant of each hybrid were determined. Leaf appearance rate was calculated using an assistant function created with global optimization through DEoptim from Package 'RcppDE' and read in the R pipeline. The leaf appearance rate was determined by plotting number of fully expanded leaves from the weekly measurements plotted against accumulated thermal time. The leaf appearance rate during the early vegetative stage is typically different from the late vegetative stage, so the regression was split into two parts, with the last four leaves set apart. Leaf appearance rates were determined from the estimated slope of a linear regression, leaf appearance rate 1 (early vegetative) and leaf appearance rate 2 (late vegetative).

The fraction of incident radiation intercepted (RI) was computed as described previously (Charles-Edwards 1982; Lafarge and Hammer 2002):

$$\text{RI} = 1 - e^{-k*\text{LAI}}$$

RI is a function of the LAI and the canopy extinction coefficient (k), which is related to canopy structure. Each day the value of LAI was computed from a sigmoidal curve as a function of leaf number, leaf appearance rate, final tiller number and leaf size distribution through accumulated thermal time, and observed canopy cover was then used to derive k based on the RI equation. To avoid any effects of senescent leaves, the canopy cover data collected after anthesis were not used for k calculation.

The RUE is defined as the quantity of dry biomass produced under non-stressed conditions based on the amount of intercepted radiation (IR). The maximum RUE for each variety was determined using the slope of the estimated linear relationship between above-ground biomass and cumulative IR, which was derived from the calculated k, calculated LAI and daily radiation.

2.7 Model validation

The APSIM models were validated using the performance trials conducted in West Lafayette, IN, in 2015 and 2017. Agricultural Production Systems sIMulator models were also validated for nine of the hybrids evaluated in multi-year trials in Bushland, TX as part of the Texas A&M Forage Sorghum Test (https://amarillo.tamu.edu/amarillo-center-programs/agronomy/forage-sorghum/). For each hybrid, there were different sowing and harvesting dates. When plant stand count was not collected, we applied 90 % germination rate to the seeding rate as the assumed plant density (Table 3). Regression was used to compare predicted and observed values and slope and intercept parameters against the 1:1 line (Piñeiro *et al.* 2008).

The validated models were used to run a long-term simulation for these hybrids from 1980 to 2017 in both locations. In the simulation, we assumed the sowing date for all years in both locations was 1 June and the plant density was 20 plants per m^2 with no irrigation in the West Lafayette simulation and with irrigation in the Bushland simulation. The simulation harvest dates were 80, 100 and 120 DAS.

3. RESULTS

3.1 Field conditions

The average maximum temperature from sowing to the end of October in 2015, 2017 and 2018 were 26.1, 26.6 and 27.1 °C, respectively. The average minimum temperatures were 13.2, 13.8 and 14.6 °C, respectively. Total precipitation from sowing date to the end of October in 2015, 2017 and 2018 was 471.9, 628.4 and 722.2 mm, respectively, and the crops did not experience water stress. 2015 and 2017 were slightly cooler and dryer years than 2018, but there were no extreme differences between the 3 years.

3.2 Calibration of APSIM models

The commercial sorghum hybrids were compared for variations in plant density, flowering date, final dry biomass and max height (Table 1). Significant variations in plant density were detected among hybrids within and between trials. These results demonstrate that plant stand count is an important parameter and should not be replaced by seeding rate. Most of the 18 hybrids flowered at ~75 DAS, except Sordan Headless, Trudan Headless, SP SS405 and RS 400x82 BMR, which exhibited substantially later flowering dates. Analyses of variation in plant height among hybrids revealed that forage sorghum hybrids were taller (average height ~200 cm) while the grain sorghum hybrids were shorter (average height ~100 cm). These differences in morphology between the two types of sorghum represent alternate ideotypes that optimize biomass production versus grain. Final dry biomass was collected on 25 August 2015 (98 DAS), 27 September 2017 (134 DAS) and 9 August 2018 (93 DAS). In all 3 years, SP SS405 exhibited the highest final dry biomass and RS 341x10 exhibited the lowest final dry biomass.

In addition to variation in plant development and productivity, the 18 sorghum hybrids also exhibited surprising variations in leaf size distribution (Fig. 1). Maximum leaf area of these hybrids ranged from 300 to 600 cm^2. SP SS405 was late-flowering and exhibited the largest maximum leaf area while SP Trudan 8 was an early-flowering type and exhibited the smallest maximum leaf area (Fig. 1; Table 1). For most hybrids, the maximum leaf size occurred close to the middle leaf of the plant (Fig. 1). However, SP Sordan Headless and SP Trudan Headless are photoperiod-sensitive and flower very late in temperate environments (120 to 138 DAS in West Lafayette, respectively; Table 1). During the data collection from 49 to 94 DAS, these two hybrids were in vegetative growth stage and produced more full-size leaves than other hybrids. While the photoperiod-insensitive hybrids exhibit a clear, bell-shaped leaf size distribution with the largest leaf in the middle of the plant, the leaf size distribution for the photoperiod-sensitive hybrids show that each hybrid achieves a near-maximum leaf size at leaf 11 or 12, then continues to produce similar-sized leaves while the plant maintains vegetative growth (Fig. 1). This pattern of development is similar to what has been observed and parameterized for the APSIM sugarcane model (Keating *et al.* 1999, 2003). Leaf size distributions show that each hybrid has a unique canopy structure.

The management practices and biophysiological characteristics of each hybrid, including sowing date, sowing depth, plant density, observed final leaf number, final tiller number, two leaf size distribution parameters, leaf number, observed canopy cover and observed biomass were input to the pipeline for the APSIM simulation. The extinction coefficients (k) of the hybrids (Fig. 2) and estimates of RUE (Table 2) indicated that, whether photoperiod-sensitive or -insensitive, forage sorghum hybrids exhibited higher RUE. For k of all 18 hybrids, please see **Supporting Information—Fig. S1**. Thus, given the same amount of solar radiation, forage sorghum can fix more CO_2 and produce more biomass per unit of land compared to dwarf or semi-dwarf grain sorghum hybrids or to sorghum-sudan hybrids used for hay production.

To evaluate the accuracy of the parameterized and calibrated models, simulated and observed traits were evaluated over years and environments. For LAI, the six hybrids shown in Fig. 3 are representative of hybrids of different types of sorghum that farmers produce. The LAI for all 18 hybrids is in the **Supporting Information—Fig. S2**. Most of the simulation lines fall within 1 SEM, except under late-season conditions, when LAI is underestimated.

Simulations of total plant biomass production and biomass partitioning into leaves, stems and panicles are shown in Fig. 4. The APSIM simulations report green stem and leaf weights; however, senesced and non-senesced leaves and stems were not differentiated in the observed data. Therefore, some leaf and stem simulation results are underestimated in the late-season data points. The simulations of senesced leaves show that the observed leaf dry biomass is close to the simulated green leaf dry biomass plus dead leaf dry biomass. The parameterized APSIM models performed well for most of the different types of sorghum; however, there are some differences between forage sorghum and grain sorghum hybrids. When we consider the stem and leaf dry biomass simulations, the simulations of grain sorghum (Fig. 4, O–R) exhibit a better fit than in the forage sorghum hybrids (Fig. 4, A–N). For the panicle dry biomass simulations, the models perform better for forage sorghum.

3.3 Validation of APSIM models

To validate the parameterized APSIM models over environments, LAI was simulated in West Lafayette using 2015 and 2017 weather data. The models performed well in both years with simulations for six of the hybrids shown in Fig. 5. Model performance of 2015 and 2017 LAI for all 18 hybrids are shown in the **Supporting Information—Fig. S3**. Leaf area index was overestimated in hybrids with later flowering dates such as SP SS405 and SP Sordan Headless.

Given these results, above-ground dry biomass production was simulated for West Lafayette, IN and Bushland, TX representing two very different production environments (Fig. 6). The P-values in the plot test the null hypothesis that the fitted line slope is not different from 1. Only SP SS405 exhibited a slope significantly lower than 1.

Table 3. The genotypes and management details in Bushland trials.

Genotype	Year	Sowing date	Harvest date	Stand count (plants per m^2)
849F	2017	6/13	10/4	16.7
849F	2016	6/8	9/15	17.8
849F	2014	6/13	9/8	22.2
849F	2011	5/19	9/2	22.2
849F	2010	5/28	9/7	22.2
849F	2009	5/28	9/9	22.2
849F	2008	5/27	9/22	22.2
849F	2007	5/30	9/25	20.0
877F	2006	5/25	10/6	28.5
HIKANE II	2016	6/8	8/27	17.8
HIKANE II	2011	5/19	9/2	22.2
HIKANE II	2009	5/28	9/16	22.2
HIKANE II	2008	5/27	9/17	22.2
HIKANE II	2007	5/30	9/25	20.0
HIKANE II	2006	5/25	9/11	26.1
HIKANE II	2005	5/25	9/8	26.7
HIKANE II	2004	5/24	9/9	26.7
HIKANE II	2003	5/21	9/5	26.7
HIKANE II	2002	5/23	8/28	26.7
NK 300	2016	6/8	9/26	17.8
NK 300	2011	5/19	9/22	22.2
NK 300	2009	5/28	10/14	22.2
NK 300	2006	5/25	9/14	25.7
NK 300	2004	5/24	9/9	26.7
NK 300	2003	5/21	9/22	26.7
NK 300	2002	5/23	9/27	26.7
Sordan 79	2006	5/25	9/14	25.4
Sordan 79	2005	5/25	9/29	26.7
Sordan 79	2004	5/24	10/13	26.7
Sordan Headless	2016	6/8	10/25	17.8
Sordan Headless	2014	6/13	10/6	22.2
Sordan Headless	2008	5/27	10/26	22.2
Sordan Headless	2006	5/25	10/6	22.5
Sordan Headless	2005	5/25	9/29	26.7
Sordan Headless	2004	5/24	10/13	26.7
Sordan Headless	2003	5/21	10/15	26.7
Sordan Headless	2002	5/23	10/11	26.7
SS405	2017	6/13	10/26	16.7
SS405	2016	6/8	10/15	17.8
SS405	2014	6/13	9/17	22.2
SS405	2011	5/19	10/6	22.2
SS405	2009	5/28	10/14	22.2
SS405	2008	5/27	10/26	22.2
SS405	2007	5/30	9/25	20.0
SS405	2006	5/25	9/28	29.1
SS405	2005	5/25	9/29	26.7
SS405	2004	5/24	9/30	26.7
SS405	2002	5/23	9/27	26.7
SS405	2000	5/24	9/27	26.7
Trudan 8	2006	5/25	8/31	23.8
Trudan 8	2005	5/25	9/1	26.7

Table 3. Continued

Genotype	Year	Sowing date	Harvest date	Stand count (plants per m^2)
Trudan 8	2004	5/24	9/9	26.7
Trudan Headless	2014	6/13	10/6	22.2
Trudan Headless	2008	5/27	10/26	22.2
Trudan Headless	2006	5/25	10/6	24.5
Trudan Headless	2005	5/25	9/29	26.7
Trudan Headless	2004	5/24	10/13	26.7
Trudan Headless	2003	5/21	10/15	26.7
Trudan Headless	2002	5/23	10/11	26.7

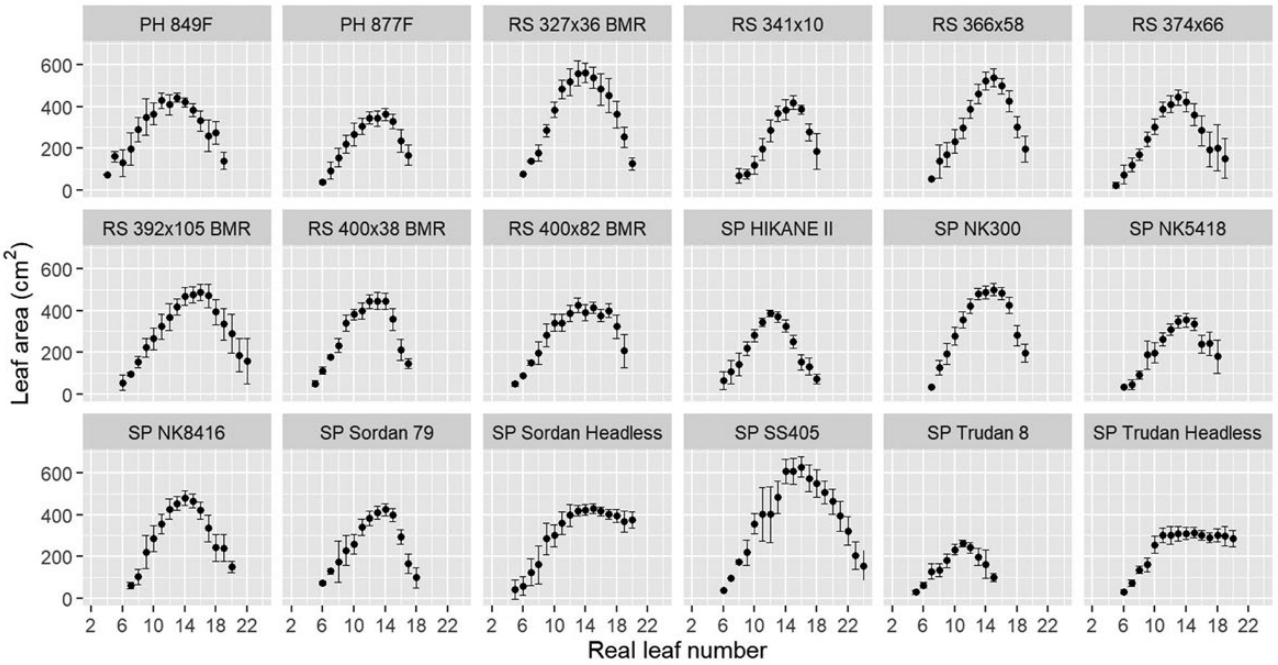

Figure 1. Leaf size distributions collected from 25 June (48 DAS), 12 July (65 DAS) and 9 August (93 DAS) at West Lafayette, IN, in 2018. Vertical bars indicate ± 1 SEM for measured values.

Given that APSIM models can simulate above-ground biomass in multiple years and different regions, the above-ground biomass for nine hybrids was simulated in West Lafayette, IN and Bushland, TX using historical weather data from 1980 to 2017. Results are shown in a biomass probability exceedance plot across years (Fig. 7). Overall, the simulated biomass in West Lafayette, IN was larger than in Bushland, TX for each of three different harvest dates. The patterns of hybrid biomass performance in the two locations differed. Considering the rank performance of hybrids, the ranks over the three harvest dates do not change much in Bushland, TX but show considerable variation from year-to-year in West Lafayette, IN. SP SS405 and the SP Sordan 79 hybrids had the highest simulated biomass, and SP Trudan Headless had the lowest biomass. Under early harvesting conditions in Bushland, TX, PH 849F, PH 877F, SP HIKANE II and SP Sordan Headless had similar simulated biomass production but indicated more variation when harvested later in the season. Plots of simulated biomass production in West Lafayette, IN showed that SP SS405 and SP Sordan 79 had highest simulated biomass yields and the SP Trudan Headless had the lowest simulated biomass at 80 DAS and 100 DAS. However, the hybrids with the highest biomass also have a large range of potential biomass. For example, SP SS405 has potential biomass between 2200 ($g\ m^{-2}$) and 3950 ($g\ m^{-2}$) at 120 DAS simulation, which has larger range than other hybrids (Fig. 7, F). SP SS405, SP Sordan 79 and SP Sordan Headless had the highest simulated biomass in West Lafayette at 120 DAS. Other hybrids exhibited a similar range of simulated biomass yields.

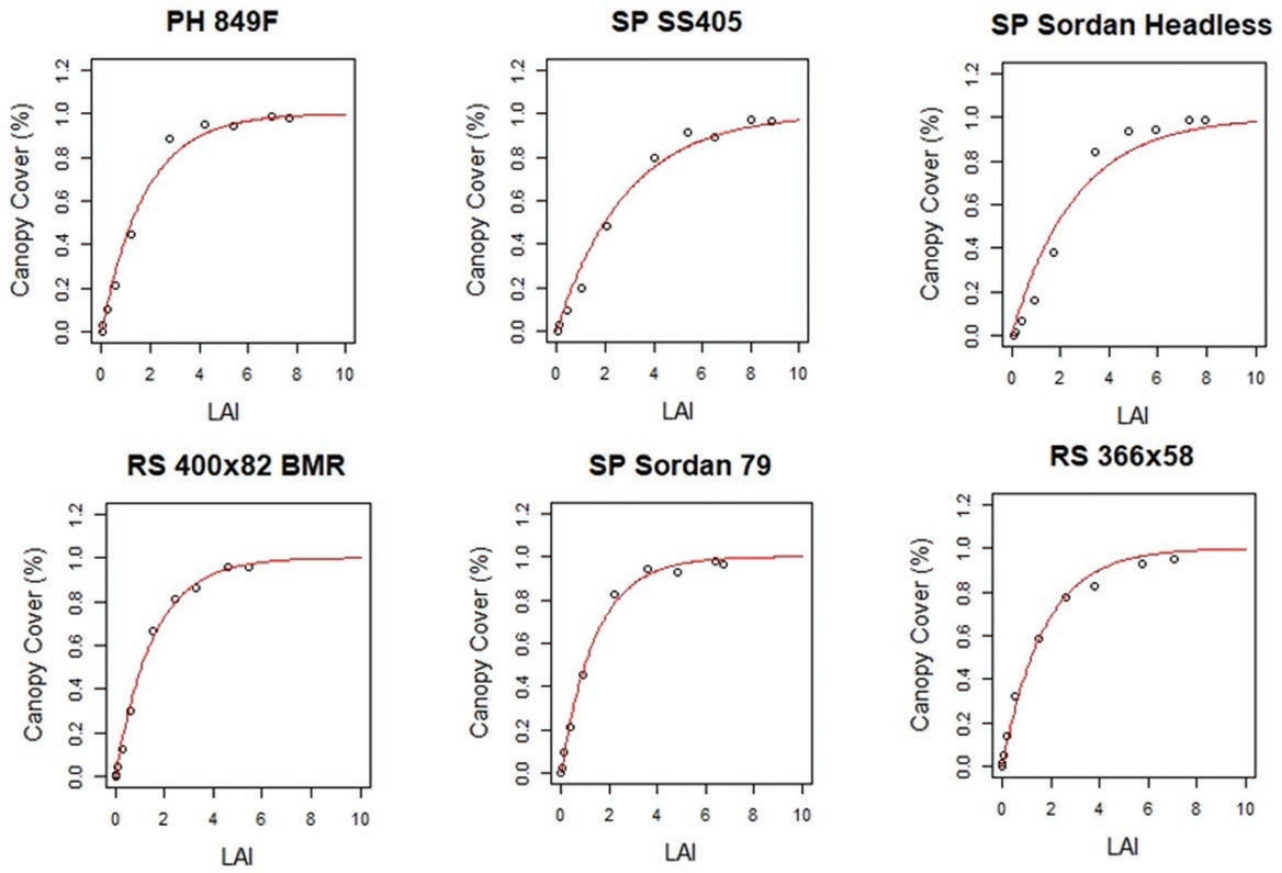

Figure 2. The canopy cover (CC) versus leaf area index (LAI) for different types of sorghum. The fitted curve ($CC = 1 - e^{-k \cdot LAI}$) indicates the extinction coefficient (k) of different types of sorghum and the values shown in Table 2.

4. DISCUSSION

4.1 Plant height and final dry biomass of photoperiod-sensitive and -insensitive forage sorghum hybrids are similar and greater than grain sorghum in medium- and short-season environments

Renewable fuels produced from plants could help to ensure future energy sustainability. Different feedstocks are used in starch-based, sugar-based and cellulose-based ethanol production. Whereas starch- and sugar-based ethanol compete with food production (Tilman *et al.* 2006), lignocellulosic biofuels do not have a potential negative influence on food production (Rubin 2008).

Not surprisingly, the yield trials and simulation studies of biomass sorghum hybrids reported in this study showed that photoperiod-sensitive and photoperiod-insensitive forage sorghum hybrids have larger max height and final dry biomass than grain sorghum. This indicates that these types of sorghum can produce more lignocellulosic biomass for ethanol and are better choices as feedstocks compared to grain sorghum. Based on our final harvest data in 2018 (Fig. 4), the proportion of stem to total biomass for forage sorghum and grain sorghum are 0.70 and 0.37, respectively. Variation in maximum height and final dry biomass of these hybrid cultivars depends on the length of the growing season. The final dry biomass of the photoperiod-insensitive forage hybrids was higher than the photoperiod-sensitive sorghum in 2018 at 94 DAS, while the photoperiod-sensitive hybrids outperformed the photoperiod-insensitive hybrids at 99 DAS in 2015 and 135 DAS in 2017 (Table 1). This is consistent with observations that the photoperiod-sensitive sorghum extends pre-floral development up to 8 months, resulting in taller plants with more leaves (Rooney 2004; Rooney *et al.* 2007; Clerget *et al.* 2008; Olson *et al.* 2012). Photoperiod-sensitive sorghum hybrids maximize the yield of lignocellulosic material not only directly through delay of reproductive growth stage but also indirectly through enhancement of drought tolerance or drought avoidance in rainfed environments (Rooney *et al.* 2007). Our results suggest that photoperiod-sensitive sorghum improves biomass production in longer growing periods by inhibiting the transition from vegetative to reproductive growth, which can add value to bioenergy production in locations that have longer growing periods with sufficiently warm temperatures.

4.2 Sorghum hybrids exhibit diverse canopy structures

In conditions of sufficient water supply, the crop biomass is determined by the accumulated radiation interception and the efficiency with which radiant energy is converted to dry matter (Monteith *et al.* 1977;

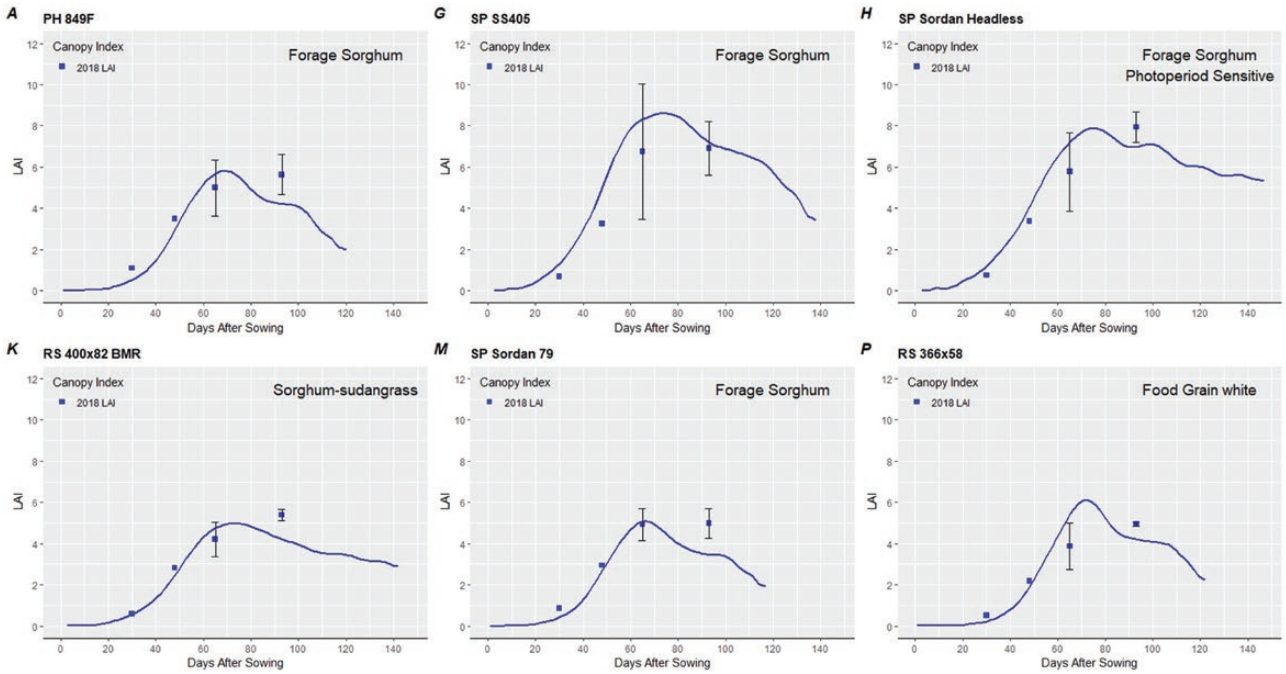

Figure 3. Simulated crop leaf area index (LAI) throughout the crop life cycle (lines) compared to measured values (symbols) for six represented hybrids of each sorghum type. The experiments were sown on 8 May 2018 at West Lafayette. Vertical bars indicate ± 1 SEM for measured values.

Muchow 1989). The amount of RI is a function of the pattern of leaf area development. Therefore, leaf size distribution is an important determinant of crop growth. In maize, Hammer *et al.* (2009) found that the change in canopy architecture may also have indirect effects via leaf area retention and partitioning of carbohydrate to the ear.

The leaf size distributions vary considerably among the hybrids reported in this study (Fig. 1). Some hybrids with larger leaf areas may produce more biomass in stress-free environments while hybrids with smaller leaf areas may perform better under drought stress. Hammer *et al.* (2009) found that crops with smaller leaf area have a yield advantage because they can reduce water use before flowering and conserve subsoil moisture that can then be accessed during the critical grain-filling period under drought stress (He *et al.* 2017). Borrell *et al.* (2014a, b) also found that the size of the crop canopy has important consequences for water use in sorghum, where the stay-green trait contributes to drought tolerance by conferring reduced tillering and smaller plant leaf areas before flowering.

Photoperiod-sensitive sorghum can achieve higher biomass when there is a longer vegetative growth supporting its potential value as a feedstock for lignocellulosic biofuel. Photoperiod-sensitive sorghum hybrids exhibit a unique pattern of leaf size distribution (Fig. 1). These hybrids remain vegetative throughout the growing season and do not produce a flag leaf or have a clear maximum leaf in the leaf size distributions. These hybrids continued growing and producing more leaves until the last harvest date in 2018 at 94 DAS. This pattern may explain why the photoperiod-sensitive sorghum had larger final dry biomass when harvested at later dates (99 DAS in 2015 and 135 DAS in 2017).

4.3 Photoperiod-sensitive and photoperiod-insensitive forage sorghum hybrids exhibit similar RUE

Radiation use efficiency is a robust and theoretically appropriate parameter for describing crop growth. The total production of dry matter is strongly correlated with intercepted solar radiation in many different species (Monteith *et al.* 1977). DeWit (1965) and Goudriaan (1982) found that RUE values are essentially stable throughout the growing season and over a wide range of production conditions for most crop species. Further analyses suggested that RUE is not particularly sensitive to leaf angle even with extreme leaf angles (Duncan 1971). Consistent with these findings, some of the hybrids in this study have relatively high extinction coefficients (k) and still have reasonable RUE (Table 2). In general, RUE is higher for C4 plants than C3 plants; Kiniry *et al.* (1989) reported the RUE for both C4 plants and C3 plants showing that C4 plants exhibited the highest RUE, with maize at 1.75 g MJ^{-1} and sorghum at 1.4 g MJ^{-1} of intercepted short-wave solar radiation. Other studies have shown maximum RUE of maize in the range 1.6–1.7 g MJ^{-1} during vegetative growth and 1.2–1.4 g MJ^{-1} for sorghum during vegetative growth, suggesting the range of potential RUE for sorghum is less than that of maize (Muchow and Davis 1988; Muchow 1989; Muchow and Sinclair 1994; Sinclair and Muchow 1999; Lindquist *et al.* 2005).

Most of the RUE studies in sorghum are for grain cultivars; however, our studies in photoperiod-sensitive and photoperiod-insensitive forage hybrids showed that these hybrids have similar RUE to one another and higher RUEs than reported for grain sorghums. Within commercial forage sorghum hybrids, the observed

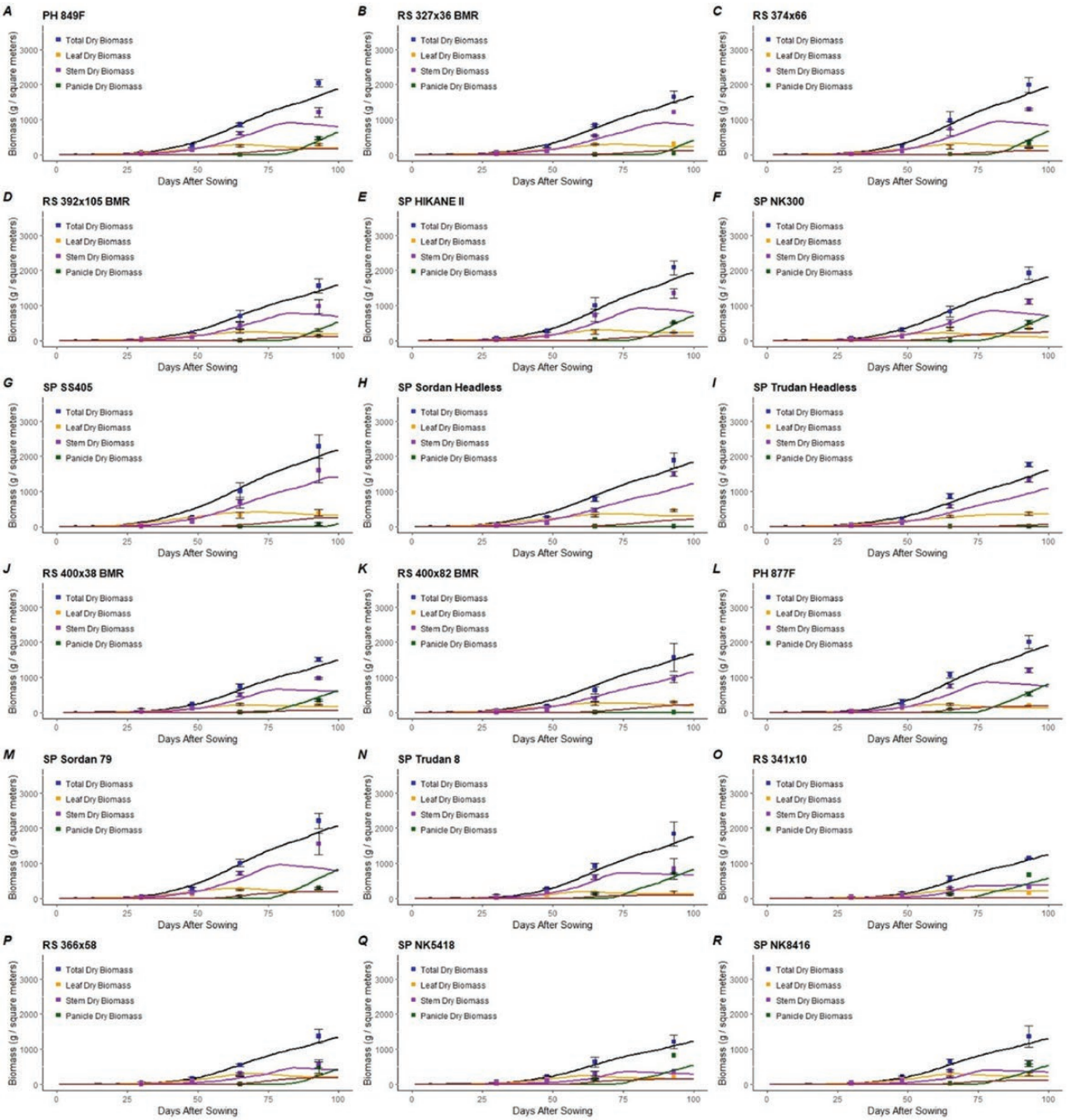

Figure 4. Simulated crop attributes throughout the crop life cycle (lines) compared to measured values (symbols) for a range of treatments for the experiments sown on 8 May 2018 at West Lafayette. Vertical bars indicate ± 1 SEM for measured values. For each forage (A–N) and grain (O–R) type hybrid, the panel shows the time course of total and organ (stem, leaf, grain) biomass. The simulated lines are in the same colour as their measured types except the simulated total dry biomass (black line) and the simulated dead leaf dry weight (brown line).

RUE ranged from 1.29 to 1.70 g MJ^{-1} with the highest RUE similar to reports in maize (Sinclair and Muchow 1999). The sorghum hybrid with highest RUE of the 18 commercial grain and biomass sorghum hybrids in our studies was SP SS405 (Table 2). This hybrid also exhibits a larger max height and greater final dry biomass. Other studies have reported similar findings of tall sorghum hybrids

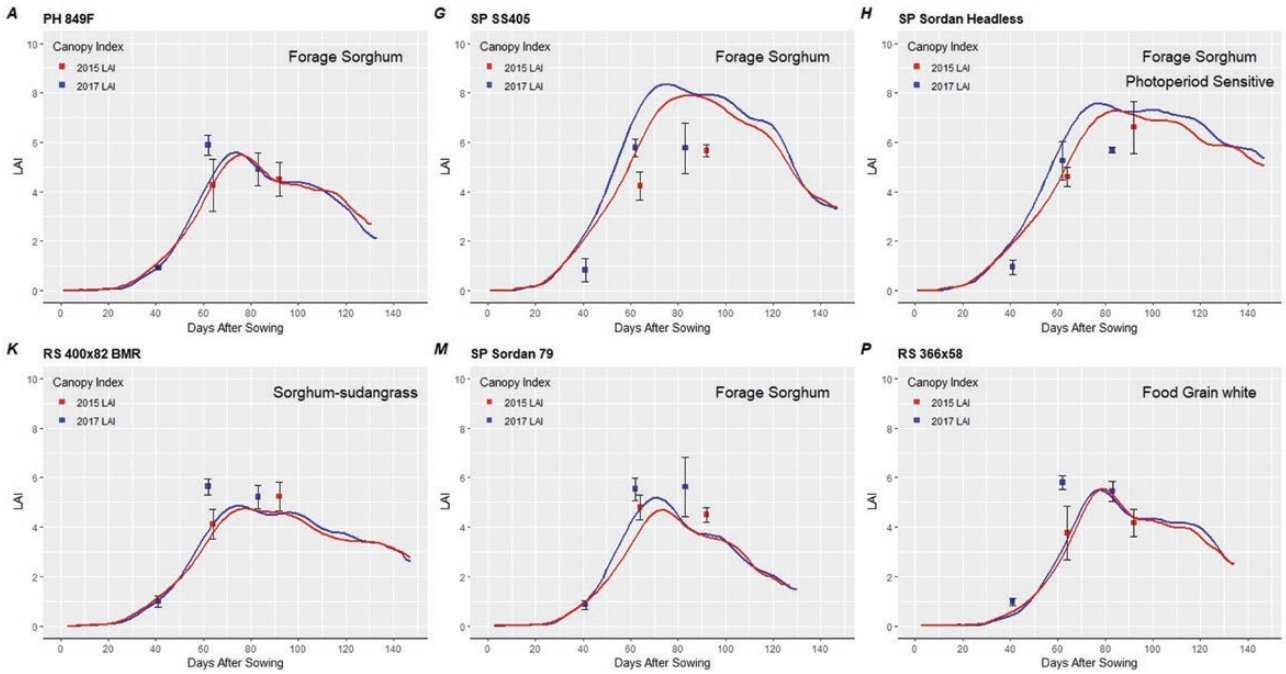

Figure 5. Simulated crop leaf area index (LAI) throughout the crop life cycle (lines) compared to measured values (symbols) for six represented hybrids of each sorghum type sown on 19 May 2015 and 16 May 2017 at West Lafayette. The simulated lines are in the same colour as their measured types. Vertical bars indicate ± 1 SEM for measured values.

exhibiting 1.65 g MJ^{-1} RUE (Hammer *et al.* 2010). Narayanan *et al.* (2013) also reported that two taller sorghum hybrids had the highest biomass and RUE in their study. Conversely, to test the hypothesis that height affects RUE in sorghum, George-Jaeggli *et al.* (2011) used dwarf sorghum to examine the effects of plant height on RUE. They found that sorghum dwarfing genes negatively affect radiation capture and in some cases RUE.

4.4 Forage sorghum models perform well in above-ground biomass simulations across years and locations

The forage and grain sorghum biomass models described in this study performed well in simulations in both West Lafayette, IN and Bushland, TX. These studies showed that the simulated above-ground biomass was higher in West Lafayette than in Bushland over multiple years. Within the set of nine hybrids evaluated at both locations, SP SS405 and SP Sordan 79 exhibited the highest RUE and simulated biomass in both locations. The photoperiod-sensitive sorghum hybrids exhibited the highest predicted biomass yields over time. Interestingly, the photoperiod-sensitive sorghum hybrids did not perform as well in Bushland as in West Lafayette. This may be because West Lafayette has comparatively higher rainfall, and the photoperiod-sensitive sorghum hybrids had more vegetative growing time to produce biomass in West Lafayette than in Bushland.

The APSIM models reported in this study can be used to explore differences in productivity among sorghum hybrids through long-term simulation. Hammer *et al.* (2014) have used APSIM to study locally optimal G × M combinations and demonstrated that significant improvements in yield and or reduction in failure risk are possible. Hammer *et al.* (2009) used the past 50 years of climate data to simulate canopy and root system architecture effects for maize that was planted at a range of densities at three representative locations throughout the US Corn Belt. Their results indicated that change in canopy architecture had little direct effect on biomass accumulation and historical yield trends, but likely had important, indirect effects via leaf area retention and partitioning of carbohydrate to the ear (Hammer *et al.* 2009).

Applying the APSIM model to sorghum can have similar benefits. White *et al.* (2015) simulated a rainfed sorghum–winter wheat rotation at Bushland, TX, from 1958 to 1999 comparing no-till versus tillage. The simulated grain sorghum biomass was lower than the one observed. Agricultural Production Systems sIMulator should also be able to improve mid-season predictions of yield. Soler *et al.* (2007) used CERES-Maize to simulate the impacts of different planting dates on four different maize hybrids under rainfed and irrigated conditions in a subtropical region of Brazil. These studies showed that an accurate yield forecast could be provided at ~45 days prior to the harvest date for all four maize hybrids (Soler *et al.* 2007). These kinds of studies are promising for farmers,

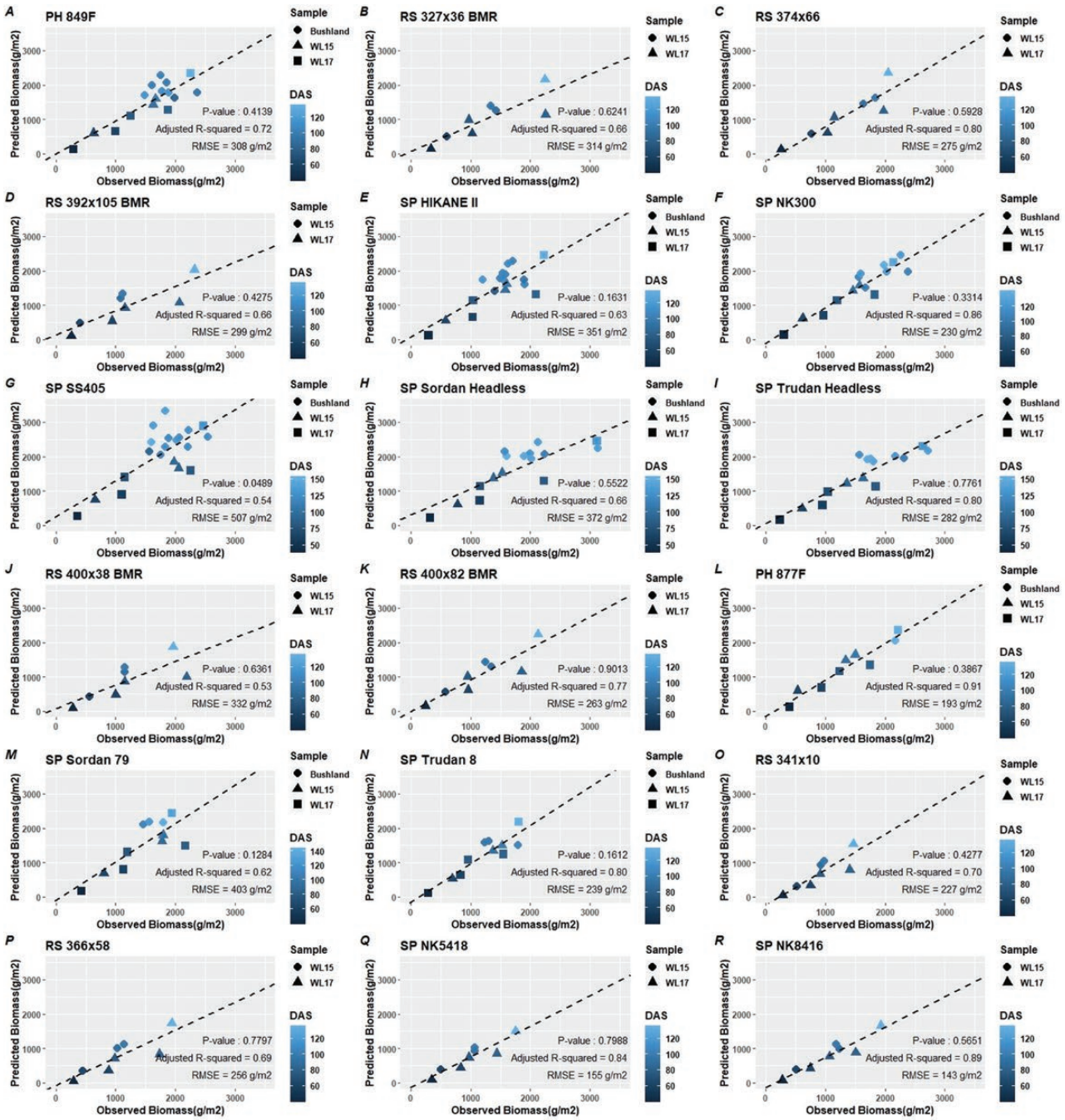

Figure 6. Model validation through comparing observed and predicted biomass of West Lafayette 2015, West Lafayette 2017 and Bushland data from 2000 to 2017. The *P*-value is to test the null hypothesis that the fitted line slope is not different from 1.

decision makers and researchers, as they could provide longer-term information for strategic management decisions, without extensive yield trials. In the future, our adapted biomass sorghum models can be applied to diverse areas and provide credible simulations for sorghum crop growth and development across a range of environments and management practices.

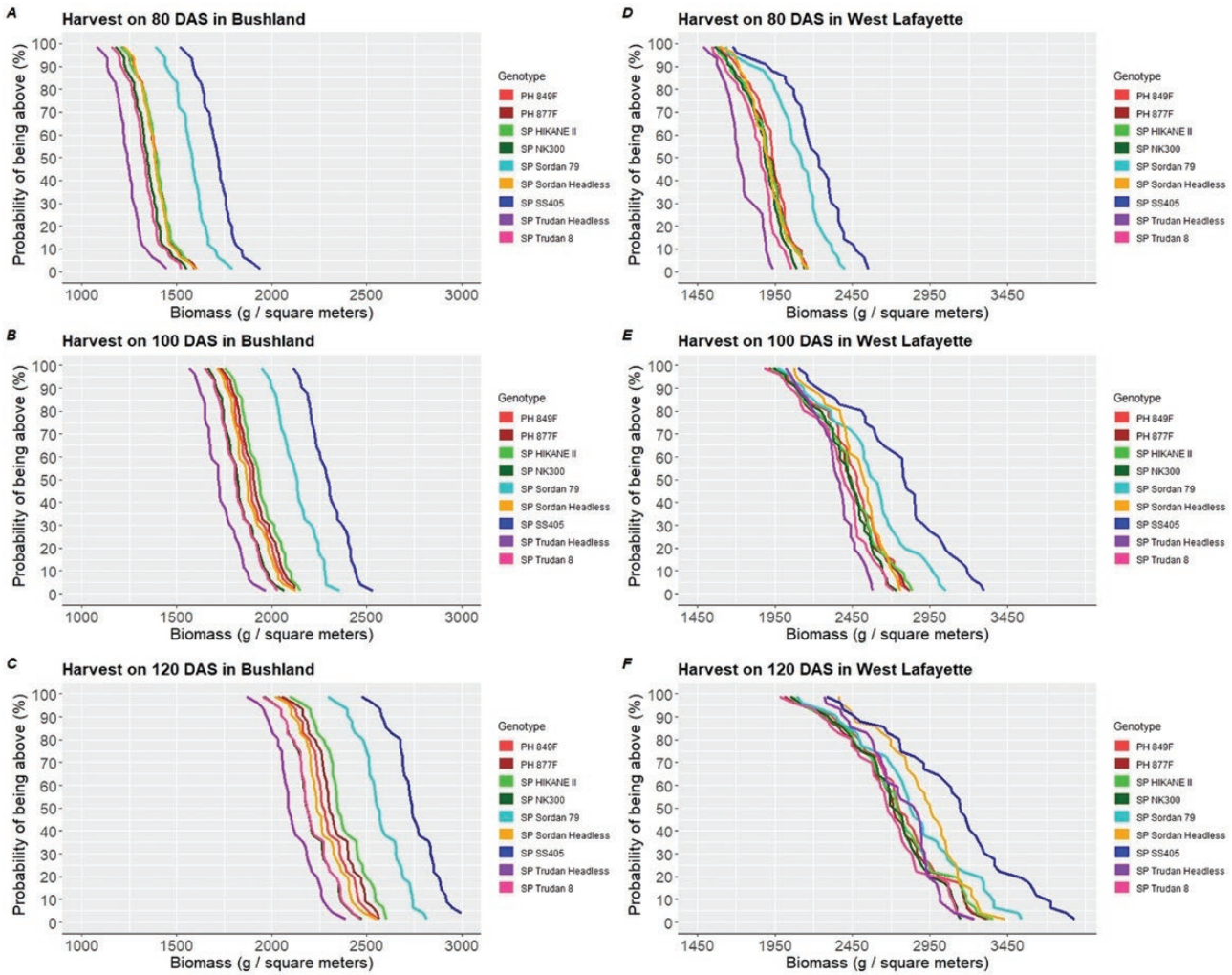

Figure 7. Biomass probability exceedance of nine hybrids from 1980 to 2017. The plots from (A) to (C) are harvested on 80, 100 and 120 DAS in Bushland, TX; the plots from (D) to (F) are harvested on 80, 100 and 120 DAS in West Lafayette, IN.

SUPPORTING INFORMATION

The following additional information is available in the online version of this article—**Figure S1.** The canopy cover (CC) versus leaf area index (LAI) for 18 sorghum hybrids. The fitted curve ($CC = 1 - e^{-k \cdot LAI}$) indicates the extinction coefficient (k) of different types of sorghum and the values shown in Table 3.

Figure S2. Simulated crop leaf area index (LAI) throughout the crop life cycle (lines) compared to measured values (symbols) for all sorghum hybrids of each sorghum type. The experiments were sown on 8 May 2018 at West Lafayette. Vertical bars indicate ± 1 SEM for measured values.

Figure S3. Simulated crop leaf area index (LAI) throughout the crop life cycle (lines) compared to measured values (symbols) for all sorghum hybrids of each sorghum type sown on 19 May 2015 and 16 May 2017 at West Lafayette. The simulated lines are in the same colour as their measured types. Vertical bars indicate ± 1 SEM for measured values.

DATA AVAILABILITY

The 'R Pipeline for Calculation of APSIM Parameters and Generating the XML File' is stored at the Purdue University Research Repository and includes the data processing pipeline, data for model input parameters and outputs comparisons, and R-codes for generating or processing central data sets (Yang *et al.* 2020a). The APSIM files used in the model calibration procedures are stored at the Purdue University Research Repository in '2018 West Lafayette Simulation of 18 Sorghum Hybrids' (Yang *et al.* 2020b). The APSIM files used for model validations are stored at the Purdue University Research Repository in the '2015 West Lafayette Simulation of 18 Sorghum Hybrids' (Yang *et al.* 2020c) and '2017 West Lafayette Simulation of 18 Sorghum Hybrids' (Yang *et al.* 2020d). The APSIM files used for the scenario simulations are stored at the Purdue University Research Repository in the 'Texas Simulation of Sorghum Hybrids Using Historical Weather Data' (Yang *et al.* 2020e) and 'West Lafayette Scenario Simulation of

Sorghum Hybrids Using Historical Weather Data' (Yang *et al.* 2020f) using multi-year historical weather data of Bushland, TX, and West Lafayette, IN.

ACKNOWLEDGEMENTS

We would like to thank the plant phenomics and crop modelling teams at Purdue University and The University of Queensland for support in agronomic trials and remote-sensing studies. We also thank Al Doherty for technical support of analyses in R and APSIM.

SOURCES OF FUNDING

This project was funded by U.S. Department of Energy ARPA-E Program Award Number DE-AR0001135.

CONTRIBUTIONS BY THE AUTHORS

K.-W. Yang contributed to data collection, data analysis and writing (original draft). S.C. contributed to conceptualization, software, writing (review & editing), supervision and methodology. N.C. contributed to data collection and data analysis. G.H. contributed to conceptualization, software and resources. G.M. and B.Z. contributed to technical support of analyses in R and APSIM. Y.C. and E.D. contributed to extraction of canopy cover from RGB images. A.M., M.C., D.E. and A.H. contributed to remote-sensing data collection and processing as well as writing (review & editing). A.T. contributed to establishment of the preliminary data collection and analysis protocol. C.W. contributed to generation of the plant materials used in this study and edited the manuscript. M.R.T. contributed to conceptualization, writing (review & editing), supervision, project administration, funding acquisition, methodology and resources.

CONFLICT OF INTEREST

None declared.

LITERATURE CITED

Baret F, Madec S, Irfan K, Lopez J, Comar A, Hemmerlé M, Dutartre D, Praud S, Tixier MH. 2018. Leaf-rolling in maize crops: from leaf scoring to canopy-level measurements for phenotyping. *Journal of Experimental Botany* **69**:2705–2716.

Blancon J, Dutartre D, Tixier MH, Weiss M, Comar A, Praud S, Baret F. 2019. A high-throughput model-assisted method for phenotyping maize green leaf area index dynamics using unmanned aerial vehicle imagery. *Frontiers in Plant Science* **10**:685.

Borrell AK, Mullet JE, George-Jaeggli B, van Oosterom EJ, Hammer GL, Klein PE, Jordan DR. 2014a. Drought adaptation of stay-green sorghum is associated with canopy development, leaf anatomy, root growth, and water uptake. *Journal of Experimental Botany* **65**:6251–6263.

Borrell AK, van Oosterom EJ, Mullet JE, George-Jaeggli B, Jordan DR, Klein PE, Hammer GL. 2014b. Stay-green alleles individually enhance grain yield in sorghum under drought by modifying canopy development and water uptake patterns. *The New Phytologist* **203**:817–830.

Bouman BAM, Keulen H van, Laar HH van, Rabbinge R. 1996. The 'School of de Wit' crop growth simulation models: a pedigree and historical overview. *Agricultural Systems* **52**:171–198.

Campbell, K. 2006. Remote sensing. In: El-Shaarawi AH, Piegorsch WW, Guttorp P, eds. *Encyclopedia of environmetrics*. John Wiley & Sons, Ltd.

Carberry PS, Muchow RC, Hammer GL. 1993. Modelling genotypic and environmental control of leaf area dynamics in grain sorghum. II. Individual leaf level - ScienceDirect. *Field Crops Research* **33**:311–328.

Casa R, Baret F, Buis S, Lopez-Lozano R, Pascucci S, Palombo A, Jones HG. 2010. Estimation of maize canopy properties from remote sensing by inversion of 1-D and 4-D models. *Precision Agriculture* **11**:319–334.

Charles-Edwards DA. 1982. *Physiological determinants of crop growth*, vol. **1**. London: Academic Press.

Chenu K, Chapman SC, Hammer GL, McLean G, Salah HB, Tardieu F. 2008. Short-term responses of leaf growth rate to water deficit scale up to whole-plant and crop levels: an integrated modelling approach in maize. *Plant, Cell & Environment* **31**:378–391.

Chenu K, van Oosterom EJ, McLean G, Deifel KS, Fletcher A, Geetika G, Tirfessa A, Mace ES, Jordan DR, Sulman R, Hammer GL. 2018. Integrating modelling and phenotyping approaches to identify and screen complex traits: transpiration efficiency in cereals. *Journal of Experimental Botany* **69**:3181–3194.

Clerget B, Dingkuhn M, Gozé E, Rattunde HF, Ney B. 2008. Variability of phyllochron, plastochron and rate of increase in height in photoperiod-sensitive sorghum varieties. *Annals of Botany* **101**:579–594.

Cobb JN, DeClerck G, Greenberg A, Clark R, McCouch S. 2013. Next-generation phenotyping: requirements and strategies for enhancing our understanding of genotype–phenotype relationships and its relevance to crop improvement. *Theoretical and Applied Genetics* **126**:867–887.

Demarez V, Duthoit S, Baret F, Weiss M, Dedieu G. 2008. Estimation of leaf area and clumping indexes of crops with hemispherical photographs. *Agricultural and Forest Meteorology* **148**:644–655.

DeWit CT de. 1965. *Photosynthesis of leaf canopies*. Wageningen, The Netherlands: Pudoc.

Diepen CA van, Wolf J, Keulen H van, Rappoldt C. 1989. WOFOST: a simulation model of crop production. *Soil Use and Management* **5**:16–24.

Duan T, Chapman SC, Guo Y, Zheng B. 2017. Dynamic monitoring of NDVI in wheat agronomy and breeding trials using an unmanned aerial vehicle. *Field Crops Research* **210**:71–80.

Duan T, Chapman SC, Holland E, Rebetzke GJ, Guo Y, Zheng B. 2016. Dynamic quantification of canopy structure to characterize early plant vigour in wheat genotypes. *Journal of Experimental Botany* **67**:4523–4534.

Duan S-B, Li Z-L, Wu H, Tang B-H, Ma L, Zhao E, Li C. 2014. Inversion of the PROSAIL model to estimate leaf area index of maize, potato, and sunflower fields from unmanned aerial vehicle hyperspectral data. *International Journal of Applied Earth Observation and Geoinformation* **26**:12–20.

Duncan WG. 1971. Leaf angles, leaf area, and canopy photosynthesis 1. *Crop Science* **11**:482–485.

Furbank RT, Tester M. 2011. Phenomics–technologies to relieve the phenotyping bottleneck. *Trends in Plant Science* **16**:635–644.

George-Jaeggli B, Jordan DR, Oosterom EJ van, Hammer GL. 2011. Decrease in sorghum grain yield due to the dw3 dwarfing gene is caused by reduction in shoot biomass. *Field Crops Research* **124**:231–239.

Gill JR, Burks PS, Staggenborg SA, Odvody GN, Heiniger RW, Macoon B, Moore KJ, Barrett M, Rooney WL. 2014. Yield results and stability analysis from the sorghum regional biomass feedstock trial. *BioEnergy Research* **7**:1026–1034.

Gouache D, Beauchêne K, Mini A, Fournier A, Solan B de, Baret F, Comar A. 2016. Applying remote sensing expertise to crop improvement: progress and challenges to scale up high throughput field phenotyping from research to industry. In: *Autonomous air and ground sensing systems for agricultural optimization and phenotyping*, vol. **9866**. Baltimore, USA: International Society for Optics and Photonics, 986604. doi:10.1117/12.2229389.

Goudriaan J. 1982. Potential production processes. In: Penning de Vries FWT, van Laar HH, eds. *Simulation of plant growth and crop production*. Wageningen: Pudoc, 98–113.

Guo W, Zheng B, Duan T, Fukatsu T, Chapman S, Ninomiya S. 2017. EasyPCC: benchmark datasets and tools for high-throughput measurement of the plant canopy coverage ratio under field conditions. *Sensors* **17**:798.

Hammer GL, Carberry PS, Muchow RC. 1993. Modelling genotypic and environmental control of leaf area dynamics in grain sorghum. I. Whole plant level - ScienceDirect. *Field Crops Research* **33**:293–310.

Hammer GL, Dong Z, McLean G, Doherty A, Messina C, Schussler J, Zinselmeier C, Paszkiewicz S, Cooper M. 2009. Can changes in canopy and/or root system architecture explain historical maize yield trends in the U.S. Corn Belt? *Crop Science* **49**:299–312.

Hammer GL, McLean G, Chapman S, Zheng B, Doherty A, Harrison MT, Oosterom E van, Jordan D. 2014. Crop design for specific adaptation in variable dryland production environments. *Crop and Pasture Science* **65**:614–626.

Hammer GL, Muchow RC. 1994. Assessing climatic risk to sorghum production in water-limited subtropical environments I. Development and testing of a simulation model - ScienceDirect. *Field Crops Research* **36**:221–234.

Hammer GL, van Oosterom E, McLean G, Chapman SC, Broad I, Harland P, Muchow RC. 2010. Adapting APSIM to model the physiology and genetics of complex adaptive traits in field crops. *Journal of Experimental Botany* **61**:2185–2202.

He J, Du Y-L, Wang T, Turner NC, Yang R-P, Jin Y, Xi Y, Zhang C, Cui T, Fang X-W, Li F.-M. 2017. Conserved water use improves the yield performance of soybean (*Glycine max* (L.) Merr.) under drought. *Agricultural Water Management* **179**:236–245.

He J, Zhao X, Laroche A, Lu Z-X, Liu H, Li Z. 2014. Genotyping-by-sequencing (GBS), an ultimate marker-assisted selection (MAS) tool to accelerate plant breeding. *Frontiers in Plant Science* **5**:484.

He F, Zhou T, Xiong W, Hasheminnasab SM, Habib A. 2018. Automated aerial triangulation for UAV-based mapping. *Remote Sensing* **10**:1952.

Holzworth DP, Huth NI, deVoil PG, Zurcher EJ, Herrmann NI, McLean G, Chenu K, Oosterom EJ van, Snow V, Murphy C, Moore AD, Brown H, Whish JPM, Verrall S, Fainges J, Bell LW, Peake AS, Poulton PL, Hochman Z, Thorburn PJ, Gaydon DS, Dalgliesh NP, Rodriguez D, Cox H, Chapman S, Doherty A, Teixeira E, Sharp J, Cichota R, Vogeler I, Li FY, Wang E, Hammer GL, Robertson MJ, Dimes JP, Whitbread AM, Hunt J, Rees H van, McClelland T, Carberry PS, Hargreaves JNG, MacLeod N, McDonald C, Harsdorf J, Wedgwood S, Keating BA. 2014. APSIM – Evolution towards a new generation of agricultural systems simulation. *Environmental Modelling & Software* **62**:327–350.

Holzworth D, Huth NI, Fainges J, Brown H, Zurcher E, Cichota R, Verrall S, Herrmann NI, Zheng B, Snow V. 2018. APSIM Next Generation: overcoming challenges in modernising a farming systems model. *Environmental Modelling & Software* **103**:43–51.

Jiang R, He W, Zhou W, Hou Y, Yang JY, He P. 2019. Exploring management strategies to improve maize yield and nitrogen use efficiency in northeast China using the DNDC and DSSAT models. *Computers and Electronics in Agriculture* **166**:104988.

Jimenez-Berni JA, Deery DM, Rozas-Larraondo P, Condon ATG, Rebetzke GJ, James RA, Bovill WD, Furbank RT, Sirault XRR. 2018. High throughput determination of plant height, ground cover, and above-ground biomass in wheat with LiDAR. *Frontiers in Plant Science* **9**:237.

Jones JW, Antle JM, Basso B, Boote KJ, Conant RT, Foster I, Godfray HCJ, Herrero M, Howitt RE, Janssen S, Keating BA, Munoz-Carpena R, Porter CH, Rosenzweig C, Wheeler TR. 2017. Brief history of agricultural systems modeling. *Agricultural Systems* **155**:240–254.

Jones JW, Hoogenboom G, Porter CH, Boote KJ, Batchelor WD, Hunt LA, Wilkens PW, Singh U, Gijsman AJ, Ritchie JT. 2003. The DSSAT cropping system model. *European Journal of Agronomy* **18**:235–265.

Keating BA, Carberry PS, Hammer GL, Probert ME, Robertson MJ, Holzworth D, Huth NI, Hargreaves JNG, Meinke H, Hochman Z, McLean G, Verburg K, Snow V, Dimes JP, Silburn M, Wang E, Brown S, Bristow KL, Asseng S, Chapman S, McCown RL, Freebairn DM, Smith CJ. 2003. An overview of APSIM, a model designed for farming systems simulation. *European Journal of Agronomy* **18**:267–288.

Keating BA, Robertson MJ, Muchow RC, Huth NI. 1999. Modelling sugarcane production systems I. Development and performance of the sugarcane module. *Field Crops Research* **61**:253–271.

Kiniry JR, Jones CA, O'Toole JC, Blanchet R, Cabelguenne M, Spanel DA. 1989. Radiation-use efficiency in biomass accumulation prior to grain-filling for five grain-crop species. *Field Crops Research* **20**:51–64.

Konare D, Pierre S, Weng JY, Morand E. 2003. Real-time image processing for remote sensing. In: *CCECE 2003 - Canadian Conference on Electrical and Computer Engineering. Toward a Caring and Humane Technology (Cat. No. 03CH37436)*, vol. **2**. Montreal, Quebec, Canada, 699–702. doi:10.1109/CCECE.2003.1225991.

Lafarge TA, Hammer GL. 2002. Predicting plant leaf area production: shoot assimilate accumulation and partitioning, and leaf area ratio, are stable for a wide range of sorghum population densities. *Field Crops Research* **77**:137–151.

Lindquist JL, Arkebauer TJ, Walters DT, Cassman KG, Dobermann A. 2005. Maize radiation use efficiency under optimal growth conditions. *Agronomy Journal* **97**:72–78.

Masjedi A, Carpenter NR, Crawford MM, Tuinstra MR. 2019. Prediction of sorghum biomass using UAV time series data and recurrent neural networks. In *Proceedings of the IEEE Conference on Computer Vision and Pattern Recognition Workshops*, Long Beach, CA, USA, 16–20.

Masjedi A, Zhao J, Thompson AM, Yang K-W, Flatt JE, Crawford MM, Ebert DS, Tuinstra MR, Hammer G, Chapman S. 2018. Sorghum biomass prediction using UAV-based remote sensing data and crop model simulation. In: *IGARSS 2018 – 2018 IEEE International Geoscience and Remote Sensing Symposium*, Valencia, Spain, 22–27 July, 7719–7722.

Monteith JL, Moss CJ, William CG, Wingate PN, Hutton BGD. 1977. Climate and the efficiency of crop production in Britain. *Philosophical Transactions of the Royal Society of London. B, Biological Sciences* **281**:277–294.

Muchow RC. 1989. Comparative productivity of maize, sorghum and pearl millet in a semi-arid tropical environment I. Yield potential. *Field Crops Research* **20**:191–205.

Muchow RC, Carberry PS. 1990. Phenology and leaf-area development in a tropical grain sorghum - ScienceDirect. *Field Crops Research* **23**:221–237.

Muchow RC, Davis R. 1988. Effect of nitrogen supply on the comparative productivity of maize and sorghum in a semi-arid tropical environment II. Radiation interception and biomass accumulation. *Field Crops Research* **18**:17–30.

Muchow RC, Sinclair TR. 1994. Nitrogen response of leaf photosynthesis and canopy radiation use efficiency in field-grown maize and sorghum. *Crop Science* **34**:721–727.

Narayanan S, Aiken RM, Vara Prasad PV, Xin Z, Yu J. 2013. Water and radiation use efficiencies in sorghum. *Agronomy Journal* **105**:649.

Olson SN, Ritter K, Rooney W, Kemanian A, McCarl BA, Zhang Y, Hall S, Packer D, Mullet J. 2012. High biomass yield energy sorghum: developing a genetic model for C4 grass bioenergy crops. *Biofuels, Bioproducts and Biorefining* **6**:640–655.

van Oosterom EJ, Carberry PS, O'Leary GJ. 2001. Simulating growth, development, and yield of tillering pearl millet: I. Leaf area profiles on main shoots and tillers - ScienceDirect. *Field Crops Research* **72**:51–66.

Parent B, Millet EJ, Tardieu F. 2019. The use of thermal time in plant studies has a sound theoretical basis provided that confounding effects are avoided. *Journal of Experimental Botany* **70**:2359–2370.

Piñeiro G, Perelman S, Guerschman J, Paruelo J. 2008. How to evaluate models: observed vs. predicted or predicted vs. observed? *Ecological Modelling* **216**:316–322.

Ravi R, Lin Y-J, Elbahnasawy M, Shamseldin T, Habib A. 2018. Bias impact analysis and calibration of terrestrial mobile LiDAR system with several spinning multibeam laser scanners. *IEEE Transactions on Geoscience and Remote Sensing* **56**:5261–5275.

Ravi Kumar S, Hammer G, Broad I, Harland P, McLean G. 2009. Modelling environmental effects on phenology and canopy development of diverse sorghum genotypes - ScienceDirect. *Field Crops Research* **111**:157–165.

Ribera J, He F, Chen Y, Habib AF, Delp EJ. 2018. Estimating phenotypic traits from UAV based RGB imagery. In: *Proceedings of the ACM SIGKDD Conference on Knowledge Discovery and Data Mining, Workshop on Data Science for Food, Energy, and Water*, August 2016, San Francisco, CA.

Rocateli AC, Raper RL, Balkcom KS, Arriaga FJ, Bransby DI. 2012. Biomass sorghum production and components under different irrigation/tillage systems for the southeastern U.S. *Industrial Crops and Products* **36**:589–598.

Rodríguez-Álvarez MX, Boer MP, van Eeuwijk FA, Eilers PHC. 2018. Correcting for spatial heterogeneity in plant breeding experiments with P-splines. *Spatial Statistics* **23**:52–71.

Rooney WL. 2004. Sorghum improvement-integrating traditional and new technology to produce improved genotypes. *Advances in agronomy* **83**:S0065–2113.

Rooney WL, Blumenthal J, Bean B, Mullet JE. 2007. Designing sorghum as a dedicated bioenergy feedstock. *Biofuels, Bioproducts and Biorefining* **1**:147–157.

Rubin EM. 2008. Genomics of cellulosic biofuels. *Nature* **454**:841–845.

Schneider CA, Rasband WS, Eliceiri KW. 2012. NIH Image to ImageJ: 25 years of image analysis. *Nature Methods* **9**:671–675.

Sieglinger JB. 1936. Leaf number of sorghum stalks1. *Agronomy Journal* **28**:636–642.

Sinclair TR, Muchow RC. 1999. Radiation use efficiency. *Advances in Agronomy* **65**:215–265.

Soler CMT, Sentelhas PC, Hoogenboom G. 2007. Application of the CSM-CERES-Maize model for planting date evaluation and yield forecasting for maize grown off-season in a subtropical environment. *European Journal of Agronomy* **27**:165–177.

Stanton C, Starek MJ, Elliott N, Brewer M, Maeda MM, Chu T. 2017. Unmanned aircraft system-derived crop height and normalized difference vegetation index metrics for sorghum yield and aphid stress assessment. *Journal of Applied Remote Sensing* **11**:026035.

Stöckle CO, Donatelli M, Nelson R. 2003. CropSyst, a cropping systems simulation model. *European Journal of Agronomy* **18**:289–307.

Tilman D, Hill J, Lehman C. 2006. Carbon-negative biofuels from low-input high-diversity grassland biomass. *Science* **314**:1598–1600.

Truong SK, McCormick RF, Mullet JE. 2017. Bioenergy sorghum crop model predicts VPD-limited transpiration traits enhance biomass yield in water-limited environments. *Frontiers in Plant Science* **8**:335.

Wallach D, Makowski D, Jones JW, Brun F. 2018. *Working with dynamic crop models: methods, tools and examples for agriculture and environment*, 3rd edn. Academic Press, 613.

Wang E, Robertson MJ, Hammer GL, Carberry PS, Holzworth D, Meinke H, Chapman SC, Hargreaves JNG., Huth NI, McLean G. 2002. Development of a generic crop model template in the cropping system model APSIM. *European Journal of Agronomy* **18**:121–140.

White JW, Alagarswamy G, Ottman MJ, Porter CH, Singh U, Hoogenboom G. 2015. An overview of CERES–sorghum as implemented in the cropping system model version 4.5. *Agronomy Journal* **107**:1987–2002.

Williams JR, Jones CA, Kiniry JR, Spanel DA. 1989. The EPIC crop growth model. *Transactions of the ASAE* **32**:0497–0511.

Williams JR, Renard KG, Dyke PT. 1983. EPIC: a new method for assessing erosion's effect on soil productivity. *Journal of Soil and Water Conservation* **38**:381–383.

Yang K, Chapman S, Tuinstra M. 2020a. R pipeline for calculation of APSIM parameters and generating the XML file. *Purdue University Research Repository*. doi:10.4231/69H7-CV75

Yang K, Chapman S, Tuinstra M. 2020b. 2018 West Lafayette simulation of 18 sorghum hybrids. *Purdue University Research Repository*. doi:10.4231/KMK0-J993

Yang K, Chapman S, Tuinstra M. 2020c. 2015 West Lafayette simulation of 18 sorghum hybrids. *Purdue University Research Repository*. doi:10.4231/0NX5-RT34

Yang K, Chapman S, Tuinstra M. 2020d. 2017 West Lafayette simulation of 18 sorghum hybrids. *Purdue University Research Repository*. doi:10.4231/6NW4-TB31

Yang K, Chapman S, Tuinstra M. 2020e. Texas scenario simulation of sorghum hybrids using historical weather data. *Purdue University Research Repository*. doi:10.4231/PRS2-AC22

Yang K, Chapman S, Tuinstra M. 2020f. West Lafayette scenario simulation of sorghum hybrids using historical weather data. *Purdue University Research Repository*. doi:10.4231/63GJ-CJ23

Zhang Z, Masjedi A, Zhao J, Crawford MM. 2017. Prediction of sorghum biomass based on image based features derived from time series of UAV images. In: *2017 IEEE International Geoscience and Remote Sensing Symposium (IGARSS)*, Fort Worth, TX, USA, 23–28 July, 6154–6157.

Zhou C, Ye H, Xu Z, Hu J, Shi X, Hua S, Yue J, Yang G. 2019. Estimating maize-leaf coverage in field conditions by applying a machine learning algorithm to UAV remote sensing images. *Applied Sciences* **9**:2389.